Fuel 184 (2016) 648–655

Contents lists available at ScienceDirect

Fuel

journal homepage: www.elsevier.com/locate/fuel

Full Length Article

In situ characterization of naphthenic corrosion of API 5L X70 steel at room temperature

Emerson C. Rios [a], Aloadir L. Oliveira [a], Alexsandro M. Zimer [a], Renato G. Freitas [a,b], Roberto Matos [a,c], Ernesto C. Pereira [a], Lucia H. Mascaro [a,*]

[a] Laboratório Interdisciplinar de Eletroquímica e Cerâmica (LIEC), Department of Chemistry, Federal University of São Carlos, 13565-905 São Carlos, SP, Brazil
[b] Grupo de Eletroquímica e Novos Materiais (GENMAT), Department of Chemistry, Federal University of Mato Grosso, 78060-900 Cuiabá, MT, Brazil
[c] Department of Chemistry, State University of Londrina, 86057-970 Londrina, PR, Brazil

HIGHLIGHTS

- The naphthenic corrosion occurred at room temperature.
- Insoluble iron naphthenate in mineral oil was formed on the steel surface.
- The use of *in situ* optical micrographs during the electrochemical experiments.
- The use of *in situ* FTIR to characterize corrosion product.
- The use of *in situ* AFM to study corrosion.

ARTICLE INFO

Article history:
Received 25 April 2016
Received in revised form 15 July 2016
Accepted 16 July 2016
Available online 25 July 2016

Keywords:
Naphthenic corrosion
Crude oil
Electrochemical noise
In situ FTIR
In situ AFM

ABSTRACT

Different *in situ* coupled techniques were used to characterize the naphthenic corrosion of API 5L X70 steel at room temperature. *In situ* optical microscopy coupled with an electrochemical noise technique indicated a general corrosion process. *In situ* AFM images showed the early formation of the corrosion product with a thickness of 600 nm after 90 min of immersion. The main regions observed in the temporal evolution of FTIR spectra are evidence of the formation of an iron naphthenate film even at room temperature.

1. Introduction

Crude oil containing high concentration of organic acids, such as naphthenic acid, HNap, is produced in different regions of the world. It has been described [1] that, under temperatures higher than 200 °C, the presence of HNap considerably increases the corrosion of steel parts in industrial production units. Therefore, equipment failure has become a critical safety and reliability issue [1–3]. HNap are generally defined as carboxylic acids with one or more saturated ring structures and long chains. Nowadays, linear carboxylic acids also found in oilfields [4,5], such as acetic acid, formic acid and propionic acid, are included in this category [6,7].

Naphthenic corrosion is commonly represented by the following reaction:

$$Fe + 2R[CH_2]_nCOOH \leftrightarrow Fe(R[CH_2]_nCOO)_2 + H_2 \quad (1)$$

where R denotes a hydrocarbon chain. Generally, the corrosion products are soluble in the oil [1,8].

In laboratories, many studies have been performed to mimic the environmental conditions that are observed during metal corrosion caused by petroleum acids in the production units [9–14], including naphthenic corrosion at high temperature [10–14]. However, a small number of papers [15,16] report this type of corrosion at room temperature which is an important issue since these are the environmental conditions where pipelines are installed.

Different methods have been used to study HNap corrosion in oil [1,9]: mass loss, galvanic current detection, electrical resistance, and electrochemical measurements [17]. On the other hand, there

* Corresponding author.
E-mail address: lmascaro@ufscar.br (L.H. Mascaro).

http://dx.doi.org/10.1016/j.fuel.2016.07.068
0016-2361/

are few studies which have been done concerning the coupling of electrochemical and other techniques such as optical microscopy, AFM or FTIR. The great advantage of coupled techniques is to follow the metallic corrosion *in situ* together with a second source of information for specific points on the surface [18–20].

Electrochemical noise current and potential fluctuations around the steady state [21] were used to investigate the corrosion under open circuit conditions. The electrochemical noise signal profile (amplitude fluctuations and shape of the transients) is related to the mechanism involved in the corrosion. Hass et al. [15] have recently studied the influence of the temperature and of the total acid number in the naphthenic acid corrosion of austenitic 316 stainless steel using a mixture of mineral oil and naphthenic acids. The electrochemical noise, ECN, was measured during 5 h. It was observed that, as the temperature or the total acid number increased, both the susceptibility of the steel to general corrosion and the incidence of localized corrosion increased, demonstrating that ECN is sensitive enough to identify corrosive changes.

Dias et al. [7] used AFM topography images to study AISI 1020 steel. The authors showed that the naphthenic corrosion in crude oil, with total acid number (TAN) of 0.44 and 4.73 mg KOH g^{-1}, changed after 15 days of exposition. For the steel samples exposed to oil with high total acid number, the appearance of an eroded area on the surface was observed; this eroded area indicates alveolar corrosion which leads to generalized corrosion.

From an experimental point of view, coupling *in situ* optical microscopy with the investigation of the corrosion in crude oil is impossible because the medium is black. However, it is possible to simulate the composition of a crude oil's hydrocarbons using mineral oil, which is transparent, enabling the application of these coupled techniques to such task. To guarantee the experimental condition found in the production units, corrosive agents are also added to the mineral oil. Besides, there is little understanding of the nature of the films that form on steel surfaces during the naphthenic corrosion. The operative corrosion mechanism does not appear to be conclusively identified yet, although some researchers suggest a chemical process. In this sense, Slavcheva et al. [1] proposed that many of the observations about corrosion by different research groups appear to conflict with each other, and that there is a need for more work to clarify the situation.

Considering the facts exposed above, this study aims to contribute to the characterization of the corrosion product formed on the API 5L X70 steel surface in the presence of organic acids (naphthenic acids, HNap, and acetic acid, HAc) diluted in mineral oil at room temperature. For this purpose we have used temporal series of *in situ* optical micrographs during the electrochemical experiments to obtain information about the development of corrosion, the predominant type of corrosion as well as its intensity. For information about the surface roughness and topography of the film as a function of time, *in situ* atomic force microscopy was also used. Finally, to investigate the chemical composition of the film formed, *in situ* Fourier transform infrared spectroscopy measurements as a function of time were performed. With the combined use of these techniques we were able to obtain important information using a different approach than those described in the literature [15,16] about naphthenic corrosion at room temperature.

2. Experimental

2.1. Materials and electrochemical measurements

The working electrodes were obtained from a pipeline API 5L X70 steel (0.048% Al, 0.14% C, 0.010% Cr, 0.010% Cu, 1.66% Mn, 0.002% Mo, 0.017% Ni, 0.007% P, 0.001% S, 0.16% Si, 0.013% Ti, 0.036% V, balance Fe in wt.%). The microstructure was analyzed using optical microscopy (OM). The metallographic sample preparation for OM observations consisted of grinding using up to 1200-grit paper, followed by polishing with a 0.3 μm aluminum oxide suspension. After polishing, the samples were cleaned with acetone and pure water and then etched. The specimens for general microscopic examinations were etched for 10 s in Nital 2.0%. The micrograph of the API 5L X70 steel metallographic sample, Fig. 1, showed approximately 75% of the ferrite phase with average

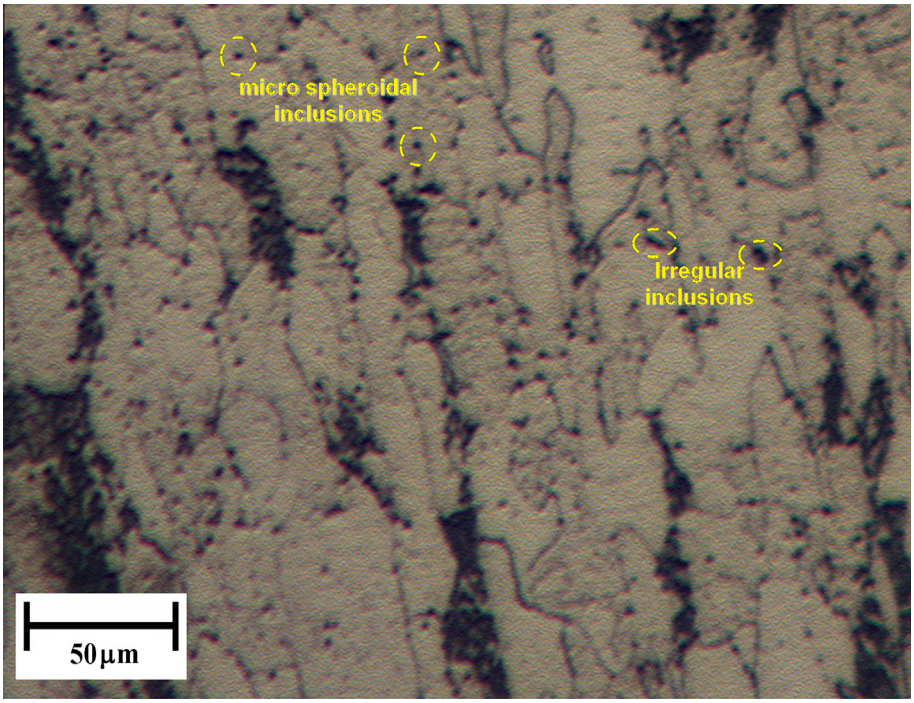

Fig. 1. Metallographic sample of API 5L X70 steel after etching with 2% Nital for 10 s.

grain size of 15 μm and elongated shape. Due to the presence of alloying elements such as Ti, V and Nb, the formation of a large number of micro-inclusions was observed. Fragiel et al. [22] investigated the chemical and microstructural characteristics of commercial API 5L X65 steel, which is very similar to the one used in our work. The authors observed a large number of micro-inclusions: about 80% spheroidals which constituted of MnS, and 20% irregular formations mainly of Ca, S and Mn compounds, with smaller amounts of Mg and C. Another common feature of this steel is that many inclusions formed by Ti_2S are distributed around the grains.

The corrosive mixture composed of organic acids and mineral oil used in all experiments was prepared by mixing HNap (Aldrich) and HAc (Merck) in mineral oil (Aldrich) under strong stirring for 20 min. The final composition was 1.5% HNap and 1.5% HAc (v/v).

For ECN measurements, two identical electrodes, WE_1 and WE_2, with A = 0.4 cm^2 were embedded in epoxy resin side by side, separated by 0.1 cm. A platinum guard ring positioned ~0.5 cm from the WE_s was used as the pseudo-reference electrode, RE. Both potential, V_n, and current, I_n, noise were collected simultaneously. In the case of V_n, it has been proposed in the literature that these values are related to the capacitance of the metal/solution interface [23]. Then, to follow the corrosion process, we decided to study only the I_n signal behavior. The analysis of I_n was performed using wavelet transform and was interpreted with energy diagram plots, EDP, which show different corrosion tendencies for the system under study.

To perform ECN measurements at E_{oc} an Autolab-PGSTAT20 with an ECN module controlled by NOVA 1.6 software was used. The measurements were performed inside a Faraday cage at room temperature (25 °C), using shielded cabling. The data was registered at a sampling frequency of f_s = 6 Hz. The signal analysis was performed using an orthogonal Daubechies function of the fourth order, "Db4", with eight levels of decomposition. The energy distribution relative to the level coefficients, d_1–d_8, reflects the information about the processes of initiation (or development) of the corrosion which are under investigation. The main property of the chosen function is that the energy of the analyzed signal is equal to the sum of the energies of all components obtained from the wavelet transform. In this work the results were interpreted by estimating the energy contribution of each level of decomposition in relation to the original signal.

2.2. In situ atomic force microscopy (AFM) studies

The corrosion processes were investigated *in situ* via atomic force microscopy using a 2100 SPM microscope (Molecular Imaging), Pico LE™ model, operated in contact mode at room temperature. A 10 μm scanner, silicon probes (Nano Sensors™) with spring constant of 0.12 N m^{-1} and a liquid cell were used. The cell was 15 mm (0.59 in.) in diameter and sealed over the sample with an o-ring. It was made from chemical-resistant polycarbonate and could be used with a wide variety of liquids. The API 5L X70 steel sample was transferred to the liquid cell filled with the oil mixture and organic acids and studied.

2.3. In situ optical microscopy coupled to electrochemical noise measurements

The electrodes were mounted in a flat-bottom electrochemical cell [19], which was positioned over the ocular of an inverted optical microscope (Opton, TNM-07T-PL model), in order to perform *in situ* image acquisition. The digital images of the WE_1 surface were collected at 100× magnification, using the software Liss View 7, with an image acquisition rate of one frame every 30 s at a resolution of 2592 × 1944 pixels. This setup allowed for optical measurements and electrochemical experiments to be performed simultaneously. All tests were performed in duplicate and the analysis of the obtained images was performed using Image-J software.

2.4. In situ Fourier transform infrared spectroscopy (FTIR) coupled to electrochemical noise measurements

In situ FTIR spectra were measured using the oil mixture with organic acids at room temperature. Spectra were collected using a Nicolet FTIR spectrometer Magna 560 equipped with a MCT detector cooled with liquid nitrogen. The spectroelectrochemical cell was home-built and fitted with a hemispherical CaF_2 window (Medway optics Ltd). The cell was vertically mounted on the lid of the sample compartment of the spectrometer in order to perform both ECN and FTIR analysis simultaneously, this setup is described with detail elsewhere [24,25]. The reflective API 5L X70 steel working electrode was mounted on a Teflon body and electrical contact was maintained by a screw and push rod arrangement, which also maintained good optical contact between the working electrode and the cell window. The angle of incidence of the IR beam (assuming 0° of beam divergence) on the CaF_2 (n = 1.41, k = 0 [26])/electrolyte interface was 46° (normal incidence at CaF_2/air interface), giving an angle of incidence at the steel electrode (assuming n = 1.33 and approximating k to 0 for water) of 51°. Even allowing for ±6° of beam spread, the incidence on the inner side of the CaF_2/-electrolyte interface is well below the critical angle, hence precluding any enhancement effects due to total internal reflectance [26]. Optical path-lengths were ca. 1.5–3 μm, giving a thin layer with thicknesses of ca. 0.8–1.2 μm. Only unpolarized light was used.

The reference spectrum (R_0) was collected at the E_{oc} and a second spectrum was taken at the same potential to check for electrode movement. Whole further spectra (R) where collected at E_{oc} with time. The spectra were calculated as the normalized difference $(R - R_0)/R_0$. Positive and negative bands represent, respectively, loss and gain of species at the sampling potential. All spectra were obtained at 256 co-added and averaged scans at 4 cm^{-1} resolution.

3. Results and discussion

It is not possible to use conventional electrochemical techniques to study the corrosion mechanism in the API 5L X70 steel in mineral oil with naphthenic acids due to the low conductivity of the solution. In this case, one method that can be used is the measurement of the electrochemical current noise during the experiment coupled with optical microscopy. This experimental setup gives information regarding the current flux (related to the amount of iron oxidized) along with visual data on the position where such reactions occur [19,27]. In the literature [28], it is proposed that the intensity of the noise is related to pit formation. Specifically, abrupt changes in the current can be explained by the local rupture of the passive layer; this is followed by repassivation that leads to a decrease in I_n to lower values. In a different manner, periodic well behaved noise curves maintaining their intensities, curve shape and frequency are attributed to generalized corrosion [15,29–32]. Fig. 2 shows the I_n signals obtained for the initial step of the corrosion of the samples here investigated in oil containing acetic and naphthenic acids.

Immediately after immersion of the steel in the corrosive environment, a transient was observed in the current signal indicating the steel corrosion process, which can be related to the presence of organic acids in the medium. The first observed values for the current were close to 10 nA which is characteristic of a low corrosion rate. This value decreased continuously and, after 552 min of experiment, the current value reached 1 nA order. One possible

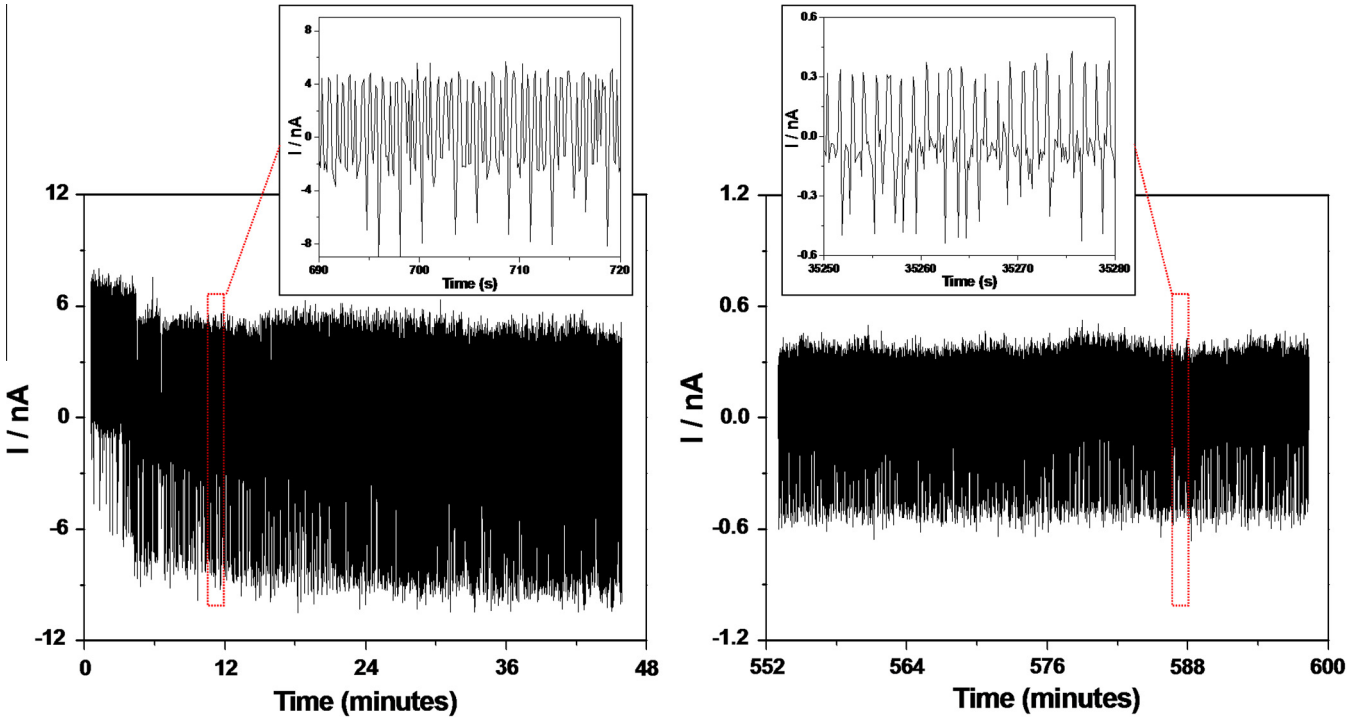

Fig. 2. Current noise of API 5L X70 steel in mineral oil + 1.5% HAc + 1.5% HNap. The inserts highlight changes in the frequency of the transients.

explanation for this behavior is the mechanism of the local dissolution and repairing of the passive film, which is expected to reach a steady state. The current fluctuation at this stage could reflect the active dissolution of the passive film, which can be regarded as general corrosion considering fingerprint criteria described in different Refs. [15,29–32]. In the present work, a regular noise pattern was observed after the immersion of the steel in the oil. However, as can be seen in the insert of Fig. 2, there is a decrease in the intensity of I_n as function of the time, and also a small change to lower frequencies. Besides papers which explain the noise results considering their shape and intensities [30], there are papers in the literature [33] which also use the accumulated energy as fingerprint criteria to discriminate between generalized and localized corrosion in electrochemical noise experiments. Al-Mazeedi and Cottis [31] described that high frequencies of events, f_n, relate to events that tend to occur all over the surface; in these cases the corrosion is, therefore, generalized. In contrast, low f_n was proposed to be related to the dissolution of large amounts of material at specific positions on the electrode and, in this case, the corrosion is localized. In this context, a high value is related to the period of the frequencies being used in the analysis. Then, if we confine the frequency range from 3 to 0.02 Hz, electrochemical transients which last 1 s can be considered fast ones. In the present case, the predominant frequency after 12 min of experiment is 1.5 Hz and after 600 min is 0.90 Hz. These frequency values are high enough to characterize generalized corrosion using the ideas proposed by Al-Mazeedi and Cottis [31].

From a different point of view, it is not easy to detect subtle changes in the time series profile. In other words, in a complex corrosion process a change in the corrosion type is difficult to be detected using only this information. However, when the data are analyzed as a function of frequency using a suitable transform, such as wavelet transform, small details become evident allowing us to relate some characteristics of the patterns with the physical chemical phenomenon of corrosion. Fig. 3 shows the diagram of the energy distribution plot, EDP, at four different times of immersion of steel in oil mixture analyzed by wavelet transform.

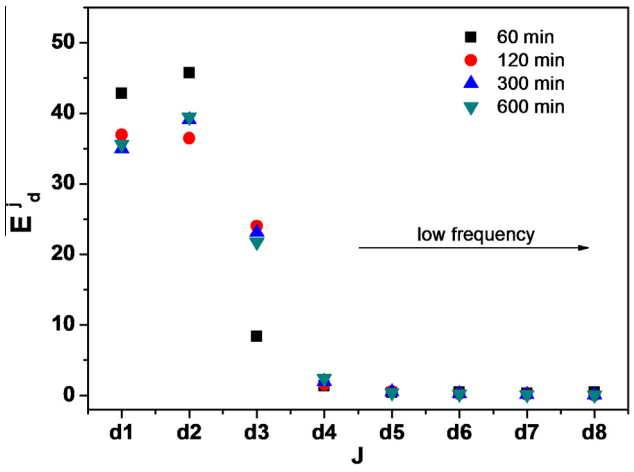

Fig. 3. Energy Distribution Plot (EDP) corresponding to ECN current signals of API 5L X70 steel in mineral oil + 1.5% HAc + 1.5% HNap.

In Fig. 3, throughout the whole experiment, it is evident that there is a predominance of accumulated energy in higher frequency levels, d_1–d_3, which are related to the general corrosion process. Also, we can see that in the time range from 0 to 1 h the process is more intense, i.e., levels d_2–d_1 store more energy in this time period.

To obtain information about the film topography during its formation, we have used *in situ* atomic force microscopy (AFM) measurements during the initial step of the experiment, until 90 min of immersion of API 5L X70 steel in oil containing HNap + HAc. It was not possible to follow the change in the topography for longer time periods using this technique due to the appearance of electronic artifacts in the data which could be correlated to the film composition. Fig. 4 shows the micrographs at different immersion times, going up to 90 min, where it is possible observe the rapid formation of a corrosion product on the metal surface. This product progressively coats most part of the surface.

After 6 min of contact of the steel with the oil solution, Fig. 4a, no corrosion product is formed. However, after 12 min, Fig. 4b, small amounts of the corrosion product are observed on the steel surface, the products progressively increase until 24 min and cover most of the surface after 60 min, Fig. 4c and d. As will be discussed in the next part of the work, with optical microscopy it is possible to follow the changes that occur in the surface during the entire experiment. In Fig. 4f, the changes in the film thickness over the sample are analyzed. Fig. 4f shows that, after 90 min, the corrosion product has a thickness higher than 500 nm, which indicates that the attack of organic acids is very strong during this initial part of the experiment. It is important to stress out that this investigation was fully carried out at 25 °C. In this sense, the presented results show that it is also possible to have naphthenic corrosion in temperatures well below those commonly studied in the literature [10,12–14], which are normally above 200 °C.

In order to investigate how deep the dissolution of iron was during the experiment we have performed a procedure. After 360 min of exposure of the sample to the corrosive environment, part of the film formed was removed from the steel surface using ultrasonic bath containing pure mineral oil and a new topographic analysis using AFM was carried out (Fig. 5). In Fig. 5a, the image obtained after the partial removal of the corrosion product is presented and, in Fig. 5b, the topographic profile plot in the same region is shown. Point A is the zero reference point, where no corrosion can be detected, and point B is the formed film. Finally, point C is a valley 75 nm below the 0 reference point, which characterizes an attacked region from which the corrosion product was removed. Then, it is possible to conclude that the formed passive film presents a lower density, comparing with the metal.

To obtain information about the chemical composition of the product formed we have used *in situ* FTIR measurements coupled with the electrochemical experiments. We have used the thin layer cell technique to obtain the IR spectra. Fig. 6 shows the FTIR spectra for the API 5L X70 immersed in mineral oil mixture for approximately 832 min. Since the changes in the spectra as a function of time can be related to changes that are occurring at the electrode/-solution interface, we can assign the downwards pointing bands to the formation of products and the bands that upwards pointing bands to the consumption of components of the oil mixture.

It is known that organic acids constitute dimers in nonpolar solvents, even at low concentrations, due to strong hydrogen bonding [34]:

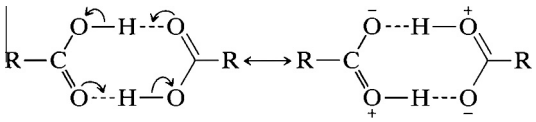

The strength of the hydrogen bonding is explained on basis of the large contribution of the ionic resonance structure. Carboxylic acid dimers display very broad and intense O—H stretching absorption in the 3300–2500 cm^{-1} region. Thus, we would expect the upward pointing band in this region to rise, due to the breakage of dimers to form iron naphthenate. However, an increase in downward pointing band is observed for a broad band between 3625 and 2990 cm^{-1}, centered at 3300 cm^{-1}. In the literature this band is related to the presence of iron carboxylates. Both acetic acid (HAc) and naphthenic acids (HNap) present the carboxyl structure. Thereby the corrosion product can be either iron acetate or iron naphthenate [35].

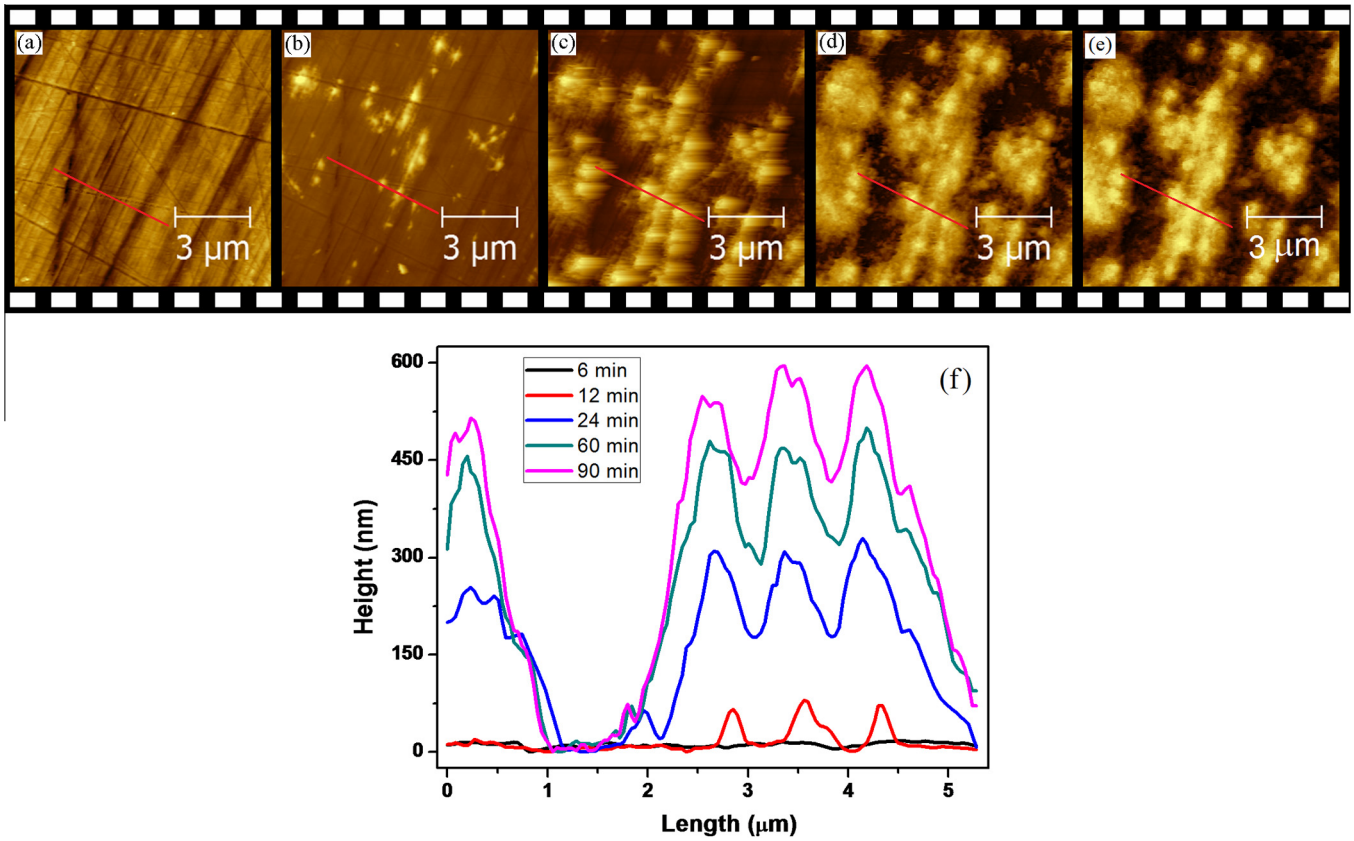

Fig. 4. *In situ* AFM images obtained during the API 5L X70 steel corrosion in mineral oil containing organic acids at room temperature after the following times of immersion: (a) 6 min; (b) 12 min; (c) 24 min, and (d) 60 min, (e) 90 min. (f) Topographic profile of the corrosion product versus time on the extension of the red line in the images. (For interpretation of the references to color in this figure legend, the reader is referred to the web version of this article.)

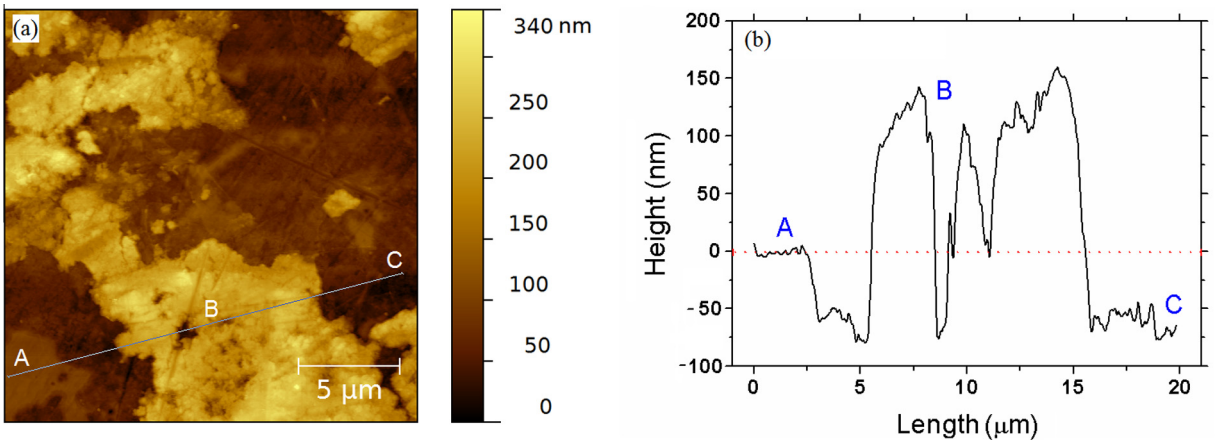

Fig. 5. (a) AFM image of a region partially covered by the corrosion film in API 5L X70 steel after 6 h of immersion in oil containing organic acids; (b) the topographic profile of this region.

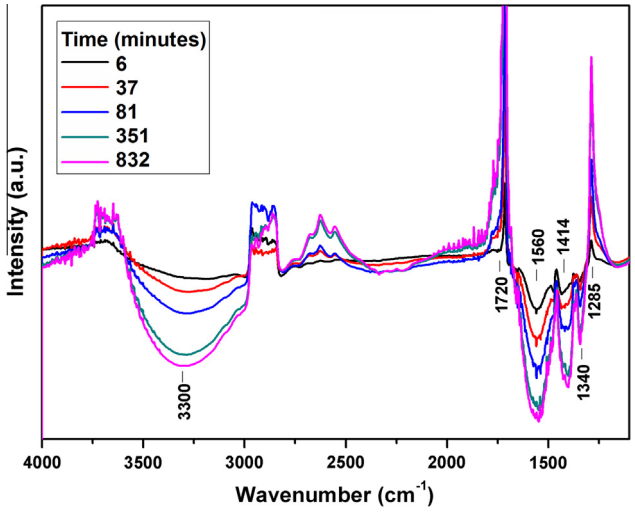

Fig. 6. *In situ* FTIR spectra of the API 5L X70 steel surface during the onset of naphthenic corrosion.

It is also presented in the literature that the role of HAc in iron corrosion is not clear. Garsany et al. [36,37] proposed that HAc can act as the cathodic reagent, which can significantly increase the rate of the cathodic reaction. From a different point of view, Crolet et al. [38] suggest that HAc acts as a weak inhibitor for the anodic dissolution reaction of iron, due to the formation of a protective film resulting from the corrosion product on the surface of the metal. Normally the pronounced effect of corrosion by HAc occurs in concentration above 10% and, in such cases, the corrosion product would be thicker. Nesic [5] studying the corrosion process in oilfield brines put the HAc as the representative of all organic acids present, i.e., HAc has a similar behavior to that of all organic acids with smaller organic chains (which tend to solubilize in the aqueous phase). Turnbull et al. [3] have also studied the influence of the size of the carbon chain on the corrosivity of naphthenic acids, verifying that longer chains lead an increase the corrosion rate. In the case of our study, we propose that the predominant component of the corrosion product is iron naphthenate, since the carbon chain of HNaps are much larger than those of HAc and their concentrations in the mineral oil is the same. Another issue to be considered is that presence of water or dissolved oxygen is practically zero in mineral oil. Therefore, only HNap and HAc are present under the experimental condition here investigated and the possibility of HAc acting in the cathodic process must be considered, as well as the formation of small quantities of iron acetate, which would be detected in the same FTIR region of iron naphthenate. In this case, iron acetate signal intensity, would be lower and, in this case, we can be attributed the broad band between 3625 and 2990 cm^{-1} to the formation of iron naphthenates:

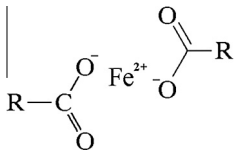

Another strong evidence of the breaking of carboxylic acid dimers is that the bands observed for 1720 and 1285 cm^{-1} rise. The band at 1720 cm^{-1} is related to C=O stretching vibrations and the one at 1285 cm^{-1} is related to the interaction between C—O stretching and in-plane C—O—H bending in the dimerized structure. The two bands that increase downward, at 1560 and 1414 cm^{-1}, also refer to the formation of iron carboxylates [35].

To summarize, the growth characteristics of the bands of naphthenic compounds, or even of hydrocarbon fractions forming the branch of these acids, are due to the formation of iron naphthenate on the electrode surface. The profile of the growth of these bands, Fig. 7, for the three major bands of the spectrum is very similar to the profile of the curve of the area covered with the corrosion product shown below in Fig. 8. Thus, together with the AFM analysis showing the appearance of a film, it is evident that the corrosion product formed on the steel is actually iron naphthenate.

To obtain information about the kinetics of the film growth we investigated the surface during the experiments in real time using optical microscopy coupled to the electrochemical noise techniques. Of course, the sensitivity of the optical microscopy technique to changes in thickness is smaller than the sensitivity of the AFM technique and this is the reason why we extended the observation period to 600 min, as presented in Fig. 4. On the other hand, as the observation spot using optical microscopy is much larger than when using AFM (Fig. 4), it is possible to conclude an increase in the covered area by corrosion products mainly until 240 min. In this case, it is important to stress out that the noise experiment is an open circuit potential technique and that, therefore, the electrode was not polarized during the experiments. The sequence of micrographs taken during the corrosion of API 5L X70 steel in oil containing organic acids, at 25 °C, is shown in Fig. 8. It is possible to follow the kinetics of the film formation and, then, the corrosion processes. In Fig. 8, the dark spots are

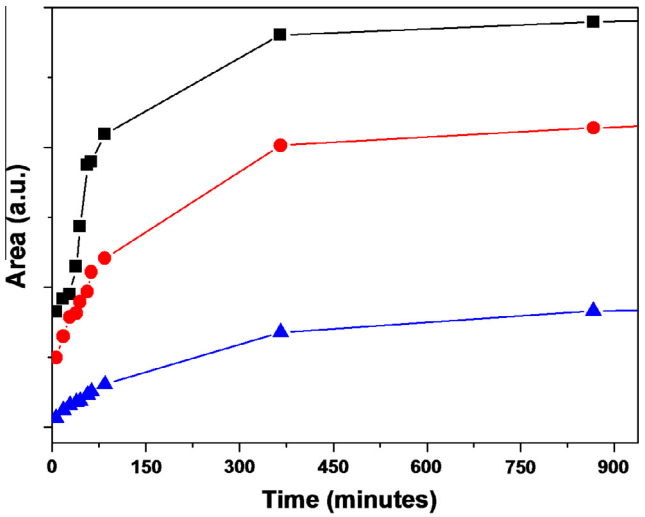

Fig. 7. The relative growth of the characteristic bands of compounds from the product of naphthenic corrosion: (■) 2969–3626 cm^{-1}, (●) 1300–1690 cm^{-1}, and (▲) 1690–1820 cm^{-1}.

related to the iron naphthenate compound formed (Fig. 6) which is above the surface (Fig. 5). After 60 min of the experiment, Fig. 8b, there is a subtle change in the texture of the image compared with the electrode at the beginning of the experiment, Fig. 8a.

The area covered by the corrosion film formed on the electrode surface was calculated during the time range in which stability was observed for the system, until about 600 min. The plot in Fig. 8f shows the covered area as function of the immersion time of the steel in the oil. Although the AFM measurement had shown that the growth rate in relation to the thickness of the film begins to stabilize after 1 h, the optical micrographs showed that a two-dimensional growth of this film is constant until approximately 5.0 h. This can be seen in the micrographs of Fig. 8c and d and in the covered area calculated plot. It is also noted that the curve has two main slopes: one at about 4 h, and another after this time. After 5 h of immersion a decrease in the dimensional growth of the film was observed. The micrograph of Fig. 8e, 10 h, shows that little change is observed when comparing to the micrograph of Fig. 8d. This behavior can be an indicative of early passivation or of the moment when all micro inclusions were converted to corrosion products.

Finally, in Fig. 8f, it is possible to observe the summary of the film formation kinetics. In this figure, it is observed that the degree of surface coverage stabilized after 240 min of experiments in a coverage value of 35% of the total area. Although we do not have a definitive explanation for this percentage, we believe that there may be a relationship between this coverage proportion and the pearlite phase of the metal (about 25%) and also the inclusions that favor the formation of corrosion product. The rate for the degree of coverage with time before 240 min was 0.17%/min.

It is well known that MnS inclusions are preferential nucleation sites during the corrosion of steel [39–41] and it was already observed that the inclusions distribution play an important role in the nucleation of the corrosion [42,43]. The data sheet of API 5L X70 steel presents that 80% of the inclusions are composed by MnS, and this is probably the cause of the onset of corrosion homogeneously along the entire surface in the form of small spots. Another point discussed here, based on the results presented, is the possible dissolution of the formed film. Many authors had reported the high solubility of iron naphthenates in oil [2,3,8,9], however here we did not observe such event. Some possible expla-

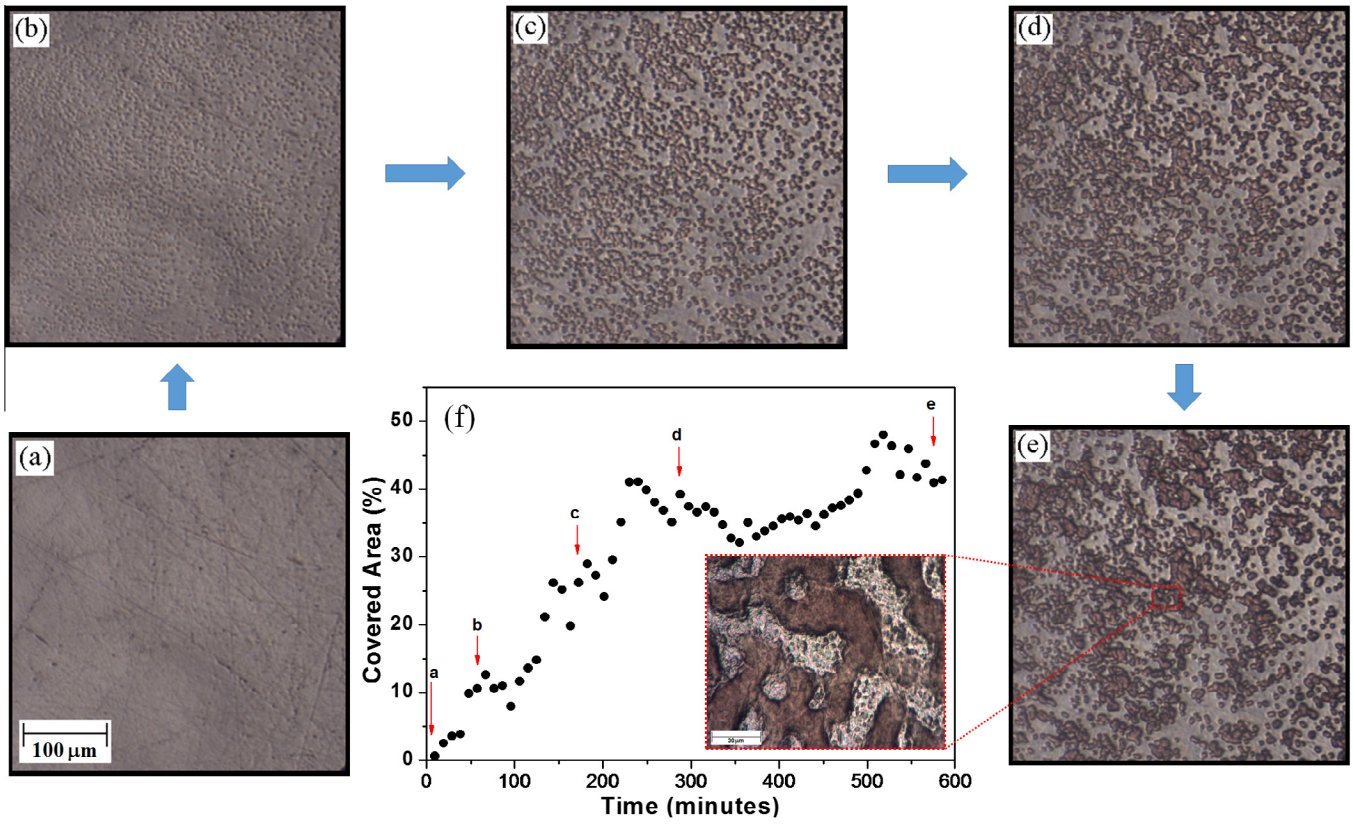

Fig. 8. Optical micrographs of the WE1 surface obtained during acquisition of ECN data. (a) t = 0.0, (b) t = 1.0, (c) t = 3.0, (d) t = 5.0, and (e) t = 10 h. In the center, covered area as a function of the time calculated from the image sequence of the corrosion process.

nations for this might be the absence of flow and the low temperature in our system. The flow together with the presence of particles in real systems of petroleum industry, besides the high temperature, would probably be the main factors that make the iron naphthenate film soluble in the oil. A second explanation would be concerning the chemical composition of our system, which does not contain sulfides. According to Yepez [2], H_2S contained in the petroleum reacts with the iron naphthenate to form FeS and naphthenic acid.

Based on the issues discussed above on iron corrosion in medium of acetic acid, the possibility of formation of iron acetate is small. Recalling that according Turnbull et al. [3] corrosivity of naphthenic acid increases with the increase in their chain length. Thus, in the current study, the greater probability is that the predominant component of the corrosion product is iron naphthenate, since the carbon chain of HNaps are much larger than those of HAc.

Finally, from the complete set of data using different techniques, it is possible to conclude the formation of a uniform film of iron naphthenate over API 5L X70 steel at room temperature which does not dissolve in the oil phase.

4. Conclusions

The initial phase of the corrosion process of API 5L X70 steel in mineral oil containing naphthenic acids, at room temperature, was characterized by different *in situ* techniques. Electrochemical noise measurements and images, obtained using optical microscopy and atomic force microscopy, allowed for the observation of the development of general corrosion, characterized by the formation of an insoluble corrosion product on the steel surface. The infrared spectra showed that this formed product is iron naphthenate. This study presented descriptions for the chemical composition of the film formed, the kinetics of its formation and allowed the proposition of general corrosion.

Acknowledgements

The authors would like to thank FAPESP (Grants No. 2013/26233-1 and No. 2011/19430-0), CEPID/FAPESP (Grant No. 2013/07296-2), CNPq and CAPES (Proc.: AUX PE-PNPD-2657/2011) for financial support. Petrobras Tranportes S.A. (TRANSPETRO) for providing the steel sample.

References

[1] Slavcheva E, Shone B, Turnbull A. Review of naphthenic acid corrosion in oil refining. Br Corros J 1999;34:125–31.
[2] Yepez O. Influence of different sulfur compounds on corrosion due to naphthenic acid. Fuel 2005;84:97–104.
[3] Turnbull A, Slavcheva T, Shone B. Factors controlling naphthenic acid corrosion. Corrosion 1998;54:922–30.
[4] Gunaltun YM, Larrey D. Correlation of cases of top of line corrosion with calculated water condensation rates. In: NACE Corrosion/2000, Orlando, Florida. Paper no. 71; 2000.
[5] Nesic S. Key issues related to modelling of internal corrosion of oil and gas pipelines – a review. Corros Sci 2007;49:4308–38.
[6] Barrow MP, Headley JV, Peru KM, Derrick PJ. Data visualization for the characterization of naphthenic acids within petroleum samples. Energy Fuels 2009;23:2592–9.
[7] Dias HP, Pereira TMC, Vanini G, Dixini PV, Celante VG, Castro EVR, et al. Monitoring the degradation and the corrosion of naphthenic acids by electrospray ionization Fourier transform ion cyclotron resonance mass spectrometry and atomic force microscopy. Fuel 2014;126:85–95.
[8] Alvisi PP, Lins VFC. An overview of naphthenic acid corrosion in a vacuum distillation plant. Eng Fail Anal 2011;18:1403–6.
[9] Zeinalov EB, Abbasov VM, Alieva LI. Petroleum acids and corrosion. Pet Chem 2009;49:185–92.
[10] Kane RD, Cayard MS. A comprehensive study on naphthenic acid corrosion. In: NACE Corrosion/2002, Houston, Texas. Paper no. 2555; 2002.
[11] Qu DR, Zheng YG, Jing HM, Yao ZM, Ke W. High temperature naphthenic acid corrosion and sulphidic corrosion of Q235 and 5Cr1/2Mo steels in synthetic refining media. Corros Sci 2006;48:1960–85.
[12] Gheorghe MB, Dingrong Q, Srdjan N, Henry AW. Naphthenic acid corrosion of mild steel in the presence of sulfide scales formed in crude oil fractions at high temperature, NACE Corrosion/2010, San Antonio, Texas. Paper no. 10353; 2010.
[13] Yu J, Jiang L, Gan F. High temperature naphthenic acid corrosion of steel in high TAN refining media. Anti-Corros Method Mater 2008;55:257–63.
[14] Wang C, Wang Y, Chen J, Sun X, Liu Z, Wan Q, et al. High temperature naphthenic acid corrosion of typical steels. Can J Mech Sci Eng 2011;2:23–9.
[15] Hass F, Abrantes ACTG, Diógenes AN, Ponte HA. Evaluation of naphthenic acidity number and temperature on the corrosion behavior of stainless steels by using electrochemical noise technique. Electrochim Acta 2014;124:206–10.
[16] Schütz P, Castilhos E, Rodrigues LM, Dick LFP. The influence of inclusions and naphthenic acids on the corrosion of pipeline steels. ECS Trans 2007;13:173–9.
[17] Yang L. Techniques for corrosion monitoring. Cambridge (England): CRC Press; 2008.
[18] Zimer AM, Rios EC, Mendes PCD, Gonçalves WN, Bruno OM, Pereira EC, et al. Investigation of AISI 1040 steel corrosion in H_2S solution containing chloride ions by digital image processing coupled with electrochemical techniques. Corros Sci 2011;53:3193–201.
[19] Rios EC, Zimer AM, Pereira EC, Mascaro LH. Analysis of AISI 1020 steel corrosion in seawater by coupling electrochemical noise and optical microscopy. Electrochim Acta 2014;124:211–7.
[20] Zimer AM, Rios EC, Pereira EC, Mascaro LH. Temporal series micrographs coupled with polarization curves to study pit formation under anodic polarization. Electrochem Commun 2011;13:1484–7.
[21] Dawson JL. Electrochemical noise measurement for corrosion applications. ASTM STP 1999;1277.
[22] Fragiel A, Schouwenaarf R, Guardián R, Pérez R. Microstructural characteristics of different commercially available API 5L X65 steels. J New Mater Electrochem Syst 2005;8:115–9.
[23] Cheng Y, Wilmott M, Luo J. The role of chloride ions in pitting of carbon steel studied by the statistical analysis of electrochemical noise. Appl Surf Sci 1999;152:161–8.
[24] Lin WF, Christensen PA, Hamnett A. In situ FTIR studies of the effect of temperature on the adsorption and electrooxidation of CO at the Ru(0 0 0 1) electrode surface. J Phys Chem B 2000;104:12002–11.
[25] Lin WF, Christensen PA, Jin JM, Hamnett A. In-situ spectroscopic studies of adsorption at the electrode and electrocatalysis. In: Sun SG, Christensen PA, Wieckowski A, editors. Amsterdam: Elsevier; 2007. p. 99.
[26] Faguy PW, Fawcett WR, Ronald W. Infrared reflection-absorption spectroscopy of the electrode/electrolyte solution interface: optical considerations. Appl Spectrosc 1990;44:1309–16.
[27] Rios EC, Zimer AM, Mendes PCD, Freitas MBJ, Castro EVR, Mascaro LH, et al. Corrosion of AISI 1020 steel in crude oil studied by the electrochemical noise measurements. Fuel 2015;150:325–33.
[28] Organ L, Scully JR, Mikhailov AS, Hudson JL. A spatiotemporal model of interactions among metastable pits and the transition to pitting corrosion. Electrochim Acta 2005;51:225–41.
[29] Aballe A, Bethencourt M, Botana F, Marcos M. Using wavelets transform in the analysis of electrochemical noise data. Electrochim Acta 1999;44:4805–16.
[30] Cheng YF, Luo JL, Wilmott M. Spectral analysis of electrochemical noise with different transient shapes. Electrochim Acta 2000;45:1763–71.
[31] Al-Mazeedi HAA, Cottis RA. A practical evaluation of electrochemical noise parameters as indicators of corrosion type. Electrochim Acta 2004;49:2787–93.
[32] Legat A, Dolecek V. Chaotic analysis of electrochemical noise measured on stainless steel. J Electrochem Soc 1995;142:1851–8.
[33] Cottis RA, Al-Awadhi MAA, Al-Mazeedi H, Turgoose S. Measures for the detection of localized corrosion with electrochemical noise. Electrochim Acta 2001;46:3665–74.
[34] Silverstein RM, Webmaster FX, Kiemle DJ. Spectroscopic identification of organic compounds. 7th ed. John Wiley; 2005. p. 95.
[35] Jang HD, Suh YJ, Kil DS, Koo KK, Kim JK, Oh HS. Preparation of iron(II) acetate powder from a low grade magnetite. US Patent 7550618 B2; 2009.
[36] Garsany Y, Pletcher D, Hedges B. Speciation and electrochemistry of brines containing acetate ion and carbon dioxide. J Electroanal Chem 2002;538:285–97.
[37] Garsany Y, Pletcher D, Sidorin D, Hedges WM. Quantifying the acetate-enhanced corrosion of carbon steel in oilfield brines. Natl Assoc Corros Eng Int: Corros J 2004;60:1155–67.
[38] Crolet JL, Thevenot N, Dugstad A, Corrosion/1999, Paper No. 24, NACE, Houston, TX; 1999.
[39] Baker MA, Castle JE. The initiation of pitting corrosion at MnS inclusions. Corros Sci 1993;34:667–82.
[40] Stewart J, Williams E. The initiation of pitting corrosion on austenitic stainless steel: on the role and importance of sulphide inclusions. Corros Sci 1992;33:457–74.
[41] Schütz P, Castilhos E, Rodrigues LM, Dick LFP. The influence of inclusions and naphthenic acids on the corrosion of pipeline steels. ECS Trans 2007;3:173–9.
[42] Webb EG, Alkire RC. Pit initiation at single sulfide inclusions in stainless steel: I. Electrochemical microcell measurements. J Electrochem Soc 2002;149: B272–9.
[43] Punckt C, Bölscher M, Rotermund HH, Mikhailov AS, Organ L, Budiansky N, et al. Sudden onset of pitting corrosion on stainless steel as a critical phenomenon. Science 2004;305:1133–6.